Simultaneous Fingerprint and High-Wavenumber Confocal Raman Spectroscopy Enhances Early Detection of Cervical Precancer In Vivo

ARTICLE *in* ANALYTICAL CHEMISTRY · JUNE 2012

Impact Factor: 5.64 · DOI: 10.1021/ac300394f · Source: PubMed

6 AUTHORS, INCLUDING:

Shiyamala Duraipandian
National University of Singapore
11 PUBLICATIONS **130** CITATIONS
SEE PROFILE

Wei Zheng
National University of Singapore
160 PUBLICATIONS **1,822** CITATIONS
SEE PROFILE

Jeffrey Low
National University of Singapore
18 PUBLICATIONS **339** CITATIONS
SEE PROFILE

Zhiwei Huang
National University of Singapore
174 PUBLICATIONS **2,446** CITATIONS
SEE PROFILE

analytical chemistry

Article

pubs.acs.org/ac

Simultaneous Fingerprint and High-Wavenumber Confocal Raman Spectroscopy Enhances Early Detection of Cervical Precancer In Vivo

Shiyamala Duraipandian,[†] Wei Zheng,[†] Joseph Ng,[‡] Jeffrey J.H. Low,[‡] A. Ilancheran,[‡] and Zhiwei Huang[†,*]

[†]Optical Bioimaging Laboratory, Department of Bioengineering, Faculty of Engineering, National University of Singapore, Singapore 117576

[‡]Division of Gynecologic Oncology, Department of Obstetrics & Gynecology, National University of Singapore and National University Health System, Singapore 119074

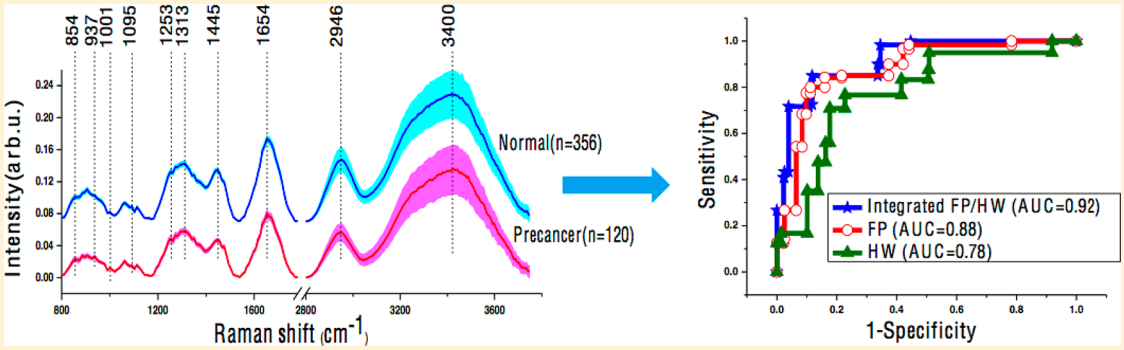

ABSTRACT: Raman spectroscopy is a vibrational spectroscopic technique capable of nondestructively probing endogenous biomolecules and their changes associated with dysplastic transformation in the tissue. The main objectives of this study are (i) to develop a simultaneous fingerprint (FP) and high-wavenumber (HW) confocal Raman spectroscopy and (ii) to investigate its diagnostic utility for improving in vivo diagnosis of cervical precancer (dysplasia). We have successfully developed an integrated FP/HW confocal Raman diagnostic system with a ball-lens Raman probe for simultaneous acquistion of FP/HW Raman signals of the cervix in vivo within 1 s. A total of 476 in vivo FP/HW Raman spectra (356 normal and 120 precancer) are acquired from 44 patients at clinical colposcopy. The distinctive Raman spectral differences between normal and dysplastic cervical tissue are observed at ~854, 937, 1001, 1095, 1253, 1313, 1445, 1654, 2946, and 3400 cm^{-1} mainly related to proteins, lipids, glycogen, nucleic acids and water content in tissue. Multivariate diagnostic algorithms developed based on partial least-squares-discriminant analysis (PLS-DA) together with the leave-one-patient-out, cross-validation yield the diagnostic sensitivities of 84.2%, 76.7%, and 85.0%, respectively; specificities of 78.9%, 73.3%, and 81.7%, respectively; and overall diagnostic accuracies of 80.3%, 74.2%, and 82.6%, respectively, using FP, HW, and integrated FP/HW Raman spectroscopic techniques for in vivo diagnosis of cervical precancer. Receiver operating characteristic (ROC) analysis further confirms the best performance of the integrated FP/HW confocal Raman technique, compared to FP or HW Raman spectroscopy alone. This work demonstrates, for the first time, that the simultaneous FP/HW confocal Raman spectroscopy has the potential to be a clinically powerful tool for improving early diagnosis and detection of cervical precancer in vivo during clinical colposcopic examination.

Cancer is an abnormal and uncontrolled cell growth that can invade and eventually destroy the surrounding healthy tissue. Although cancer can devastate many organs of the body, the incidences of breast, endometrial, ovarian, and cervical malignancies play a prominent role in overall female cancers. Cervical cancer is the second most common malignancy among women in developing countries and the seventh most common cancer in developed countries.[1,2] Accurate detection and localization of early lesions, together with effective therapeutic interventions, is crucial to increasing the survival rate of patients afflicted with cervical cancer. Currently, Papanicolaou (Pap) smear and colposcopy are the regular screening and diagnostic techniques for dysplasia and cancer of the uterine cervix, but these clinical techniques have inherent false positives and negatives.[2−5] Random biopsy sampling associated with tissue histopathology remains the gold standard approach for precancer and cancer diagnosis, but it is invasive and impractical for screening patients who may have multiple suspicious lesions.

In recent years, optical spectroscopic techniques such as reflectance, fluorescence, and Raman spectroscopy have been comprehensively investigated for precancer and cancer diagnosis in various organs including in the cervix.[6−14] In particular, near-infrared (NIR)-excited Raman spectroscopy which measures the inelastic light scattering processes in the NIR range has excelled

Received: February 9, 2012
Accepted: June 8, 2012
Published: June 20, 2012

   dx.doi.org/10.1021/ac300394f | *Anal. Chem.* 2012, 84, 5913−5919

in early detection of precancer and cancer in biomedical tissues.[9−12,14−16] NIR Raman spectroscopy has shown great promise to be a clinically diagnostic tool, because water absorption is weaker and tissue autofluorescence (AF) interference is also relatively smaller in the NIR region, compared to the ultraviolet (UV)−visible−excited Raman spectroscopy. Currently, Raman research in diagnosing precancer and cancer tissues are mostly focused on the spectral region between 800 and 1800 cm^{-1}, which is the so-called "fingerprint (FP) region" containing rich tissue biochemical information.[10−12,15−19] However, the strong tissue AF background and fiber-silica Raman signals severely interfere with the detection of the inherently weak tissue Raman signal, leading to complex fiber probe filtering design as well as signal analysis in the FP region.[20−22] On the other hand, high-wavenumber (HW) (2800−3700 cm^{-1}) Raman spectroscopy can also provide complementary biochemical information for tissue diagnosis and characterization with stronger tissue Raman signals but greatly reduced tissue autofluorescence and fiber Raman background,[14,20−23] compared to the FP Raman spectroscopy. To date, the combination of the FP and HW Raman spectroscopic techniques for disease diagnosis in the cervix has not been reported in the literature. In this work, we developed a simultaneous FP/HW confocal Raman spectroscopic system for in vivo tissue Raman measurements in the cervix. We further evaluated the diagnostic utility of the integrated FP/HW confocal Raman spectroscopy for improving in vivo cervical dysplasia detection. Multivariate statistical techniques, including partial least-squares-discriminant analysis (PLS-DA), were employed to translate the FP/HW Raman spectral differences between the normal and dysplastic tissue into diagnostically useful information for effective tissue classification.

MATERIALS AND METHODS

Confocal Raman Instrumentation. Figure 1 shows the schematic of the simultaneous FP/HW confocal Raman spectroscopy system developed for in vivo cervical Raman measurements during clinical colposcopy. The system consists of a 785-nm diode laser (100 mW, B&W TEK Inc., Newark, DE), a high-throughput spectrometer (QE65000, Ocean Optics, Inc., Dunedin, FL), an NIR-enhanced back-thinned charge-coupled device (CCD) detector (1024 × 58 with pixel sizes of 24.6 μm, QE > 90%, Hamamatsu, Shizuoka, Japan), and a custom designed hand-held confocal Raman probe with an NIR-coated sapphire ball lens (5 mm in diameter, refractive index n = 1.77) mounted on the probe tip that can effectively collect the scattered tissue Raman signal from the epithelial tissue. The ball-lens bifurcated fiber-optic confocal Raman probe consists of two fibers: one excitation fiber (200 μm, NA = 0.22) coated with a narrow band-pass filter (centered at 785 nm, fwhm = ± 2.5 nm) on the fiber tip for laser excitation, and the collection fiber (200 μm, NA = 0.22) coated with a long pass filter (cutoff at 800 nm) on the fiber tip for collecting scattered tissue Raman signal. The coupling of an NIR-coated sapphire ball lens (NA = 1.5) with the bifurcated fiber Raman probe offers a good confocality for selective collection of backscattered tissue Raman photons from the epithelial tissue (of ∼160 μm) in the cervix based on Monte Carlo simulations.[21,24] All the optics of the ball-lens Raman probe is sealed into the stainless steel sleeve (outer diameter of 8 mm) with a polytetrafluoroethylene jacket. The collected tissue Raman photons are fed into the spectrometer equipped with a customized grating and a CCD detector. The grating diffracts the incoming light and the CCD produces a digital response by converting the wavelength of Raman scattered light into a digital signal. This customized grating has the diffraction efficiency of ∼80% in the NIR region (800−1200 nm) and allows the in-house built integrated Raman system to cover both the FP (800 to 1800 cm^{-1}) and HW (2800 to 3700 cm^{-1}) analyses simultaneously for tissue Raman measurements. After the selection of required starting wavelength for spectral acquisition, the grating was permanently fixed to eliminate mechanical drifts. The detector can be cooled to −20 °C with an on-board thermoelectric cooler to reduce dark noise. The combination of the spectrometer's low-noise detector and a 16-bit A/D converter provides a signal-to-noise ratio (S/N) of 1000:1. The entire control of Raman spectroscopy system is implemented by a personal computer. The atomic emission lines of mercury−argon spectral calibration lamps (HG-1 and AR-1, Ocean Optics, Inc., Dunedin, FL) are used for wavelength calibration. All wavelength-calibrated spectra were corrected for the wavelength dependence of the system, using a tungsten-halogen calibration lamp (RS-10, EG&G Gamma Scientific, San Diego, CA). The Raman spectroscopy system with a spectral resolution of ∼8 cm^{-1} can simultaneously acquire FP (800−1800 cm^{-1}) and HW (2800−3700 cm^{-1}) tissue Raman spectra within an integration time of 1 s.

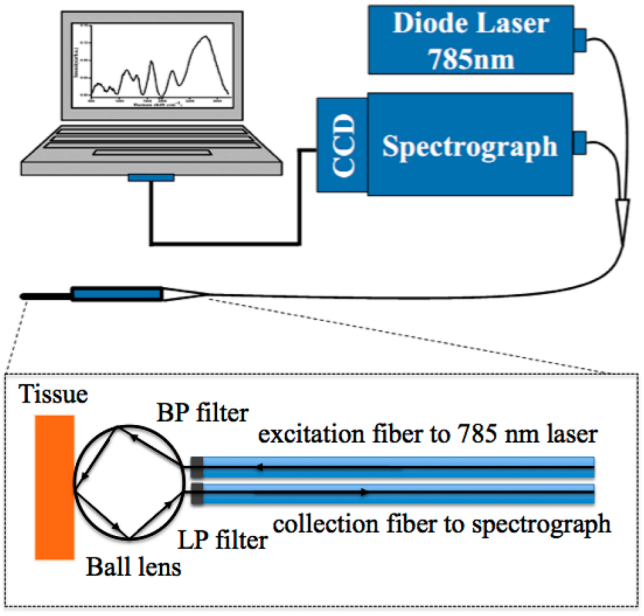

Figure 1. Schematic of the integrated FP/HW Raman spectroscopy system coupled with a ball-lens confocal Raman probe for in vivo Raman measurements on the cervix at colposcopy. (BP, band-pass; LP, long pass.)

Patients. This study protocol was approved by the Institutional Review Board (IRB) of the National Healthcare Group (NHG) of Singapore. A total of 44 nonpregnant female patients (between 18 and 70 years of age) who underwent a colposcopy procedure due to an abnormal Pap smear were recruited for Raman studies. A written informed consent form was signed by each patient before Raman spectroscopic measurements were obtained. Prior to the in vivo tissue Raman spectral measurements, a 5% acetic acid solution was applied topically on the cervix for 2 min for evaluation of the color whitening in the tissue (the degree of white discoloration in the cervix is related to the grade of precancer).[25] The application of acetic acid developed a sharp border between the normal and

dx.doi.org/10.1021/ac300394f | Anal. Chem. 2012, 84, 5913−5919

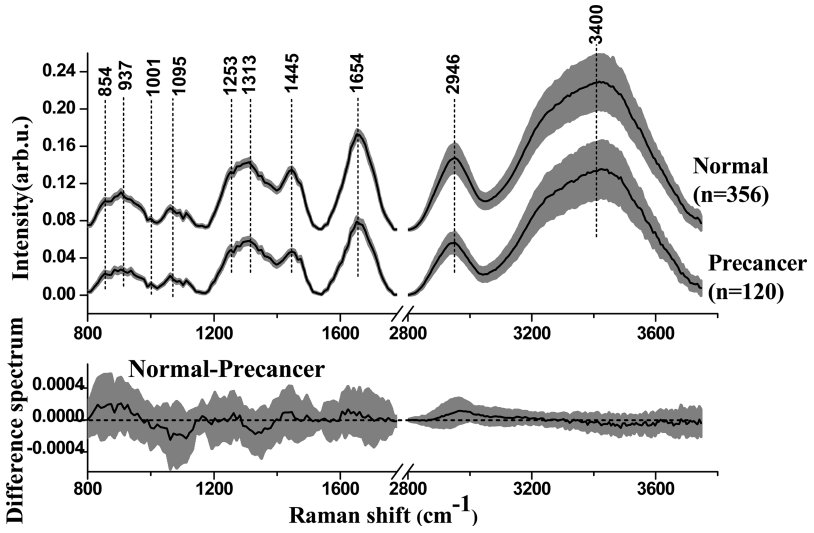

Figure 2. (a) Mean in vivo FP/HW Raman spectra ±1 standard deviation (SD) of normal (n = 356) and precancer (n = 120) cervical tissue. The mean in vivo Raman spectra of normal cervical tissue are shifted vertically for better visualization. (b) The corresponding mean difference spectra ±1 SD calculated from the mean precancer (n = 120) and normal (n = 356) cervical tissue spectra. The shaded areas represent the respective standard deviations. The broken interval (—//—) indicates the region of 1800−2800 cm^{-1}, which does not contain tissue biochemical information.

abnormal epithelium. Subsequently, the Raman spectral measurements were taken from the abnormal sites of the cervix as well as from the surrounding normal tissue sites in colposcopists' opinions (i.e., normal tissue does not exhibit color patterned changes that only accompany dysplastic epithelium).[21] To include the intra/intersubject variations for data analysis, multiple Raman spectra (∼5−8 spectra) were collected from each tissue site. As a result, a total of 476 in vivo Raman spectra (356 normal and 120 dysplasia) were collected from the 44 patients recruited. After the Raman spectral acquisition, tissue biopsies were taken from the abnormal tissue sites measured and sent for histopathology confirmation. The histopathology results served as the gold standard for the assessment of diagnostic sensitivity and specificity of the integrated in vivo FP/HW confocal Raman spectroscopy for dysplasia classification in the cervix.

Data Preprocessing. The cervical tissue Raman spectra were simultaneously acquired in the spectral range of 800−3700 cm^{-1}, but analyzed in the FP (800−1800 cm^{-1}) and HW (2800−3700 cm^{-1}) regions separately, and also in combination. The region (1800−2800 cm^{-1}) was eliminated due to the absence of biochemical information of tissue. The measured raw Raman spectra consisted of tissue AF background and weak tissue Raman signals, hence a high-order polynomial was used to describe the broad fluorescence line shape.[9] A fifth-order and a first-order polynomials provided the best fit in the FP and HW regions, respectively.[12,21,26] The polynomials were then subtracted from the noise-smoothed raw Raman spectrum to yield the tissue Raman signal alone. The background-subtracted Raman spectra were further normalized to an integrated area under the curve belonging to their respective spectral ranges (FP or HW) for standardizing the absolute tissue Raman intensities.[11,12,21]

Multivariate Analysis. The high-dimensional FP, HW, and integrated FP/HW Raman spectral space will lead to computational complexity as well as inefficiency in optimization and implementation of classification algorithms. Principal component analysis (PCA) was widely used to reduce the spectral dimension by extracting a set of principal components accounting for maximum spectral variations for tissue disease diagnostics. However, the use of partial least-squares-discriminant analysis (PLS-DA), the regression extension of PCA, would be beneficial for spectroscopic tissue diagnostics by providing group affinity (class membership of zeros and ones) information to maximize the variations between groups of samples. PLS-DA follows the principle of PCA, but further rotates the components (latent variables, LVs) to achieve the maximum group separation.[27,28] Hence, the LVs could explain the diagnostic relevant variations rather than the significant differences in the dataset. The performance of the PLS-DA diagnostic algorithm was validated in an unbiased manner using leave-one patient-out, cross-validation method. The receiver operating characteristic (ROC) curves were generated to further compare the performance of the PLS-DA models using the three spectral data sets (FP, HW, and integrated FP/HW) for in vivo diagnosis of cervical precancer.

3. RESULTS

Figure 2a shows the comparison of in vivo mean FP/HW Raman spectra ±1 standard deviation (SD) of normal (n = 356) and precancerous (n = 120) cervical tissues. The normal and precancerous cervix tissue spectra showed prominent Raman vibrational bands at ∼854 (glycogen ((CCH) deformation−aromatic) and (C−C) stretching of structural protein and collagen), ∼937 (ν(C−C) stretching of proline, valine, and glycogen), ∼1001 ((C−C) ring breathing of phenylalanine), ∼1095 (phospholipids and nucleic acids), ∼1253 (amide III), ∼1313 (CH_3CH_2 twisting mode of lipid/protein (collagen)), ∼1445 (CH_2 bending mode of proteins and lipids), ∼1654 (amide I band − (C═O) stretching mode of proteins), ∼2946 (proteins − CH_3 stretching), and ∼3400 cm^{-1} (water−(OH) stretching), respectively.[9,12,14,17,18,21,29−31] The tentative assignments of biochemicals corresponding to major Raman bands observed in normal and precancer cervical tissues are listed in Table 1. The comprehensive biomolecular basis of in vivo FP and HW Raman spectroscopic diagnosis of cervical dysplasia has been described elsewhere.[9,10,15,20,21] Figure 2b shows the difference spectra, reflecting the molecular changes in the tissue

dx.doi.org/10.1021/ac300394f | Anal. Chem. 2012, 84, 5913−5919

Table 1. Tentative Assignments of Prominent Raman Bands Identified in Normal and Precancer Cervical Tissue

peak position (cm^{-1})	vibrational mode assignment[a]	intensity change with precancer progression[b]
854	δ_d(CCH) glycogen ν(C−C) protein and collagen	−
937	ν (C−C) proline and valine, glycogen	−
1001	(C−C) ring breathing of phenylalanine	+
1095	$\nu(PO_2^-)$ nucleic acids and phospholipids ν(C−C) phospholipids	+
1253	amide III(α-helix)	−
1313	CH_3CH_2 twisting mode of protein (collagen)/lipid CH_3CH_2 wagging proteins	+
1445	$\delta(CH_2)$ proteins and lipids	−
1654	ν(C═O) amide I(α-helix)	−
2946	$\nu(CH_3)$ proteins	−
3400	ν(OH) water	+

[a] ν = stretching mode, δ_d = deformation, δ = bending mode. [b] The increase (+) or decrease (−) of mean Raman intensity associated with precancer progression.

associated with dysplastic progression. For instance, the dysplastic cervical tissue spectra increases significantly at 1001, 1095, 1313, and 3400 cm^{-1}, but exhibit much lower signal at 854, 937, 1253, 1445, 1654, and 2946 cm^{-1} as compared to the normal tissue (unpaired 2-sided Student's t-test ($p < 0.05$)).[9,12,14,18,21,29−32] The significant increase or decrease of some specific biomolecules in cervical dysplastic tissue prove the diagnostic utility of the integrated FP/HW confocal Raman spectroscopy for in vivo identification of premalignant cervical lesions at colposcopy.

To improve the tissue Raman diagnosis, these elusive biochemical differences observed in the spectra of different tissue types were explored in detail using PLS-DA multivariate algorithm. The in vivo FP, HW, and integrated FP/HW Raman spectral datasets were mean-centered to eliminate common variance.[27] The leave-one-patient-out, cross-validated PLS-DA diagnostic models were further developed for FP, HW and integrated FP/HW Raman spectral data sets using the optimum number of components (3 LVs, 1 LV, and 3 LVs (see Figure 3)), accounting for 43.43%, 27.99%, and 38.77% of total Raman spectral variations, respectively, for identifying dysplastic cervical tissue. The optimum number of components was estimated based on the local minimum of cross-validation classification error values.[28] For instance, the optimum number of components for an integrated FP/HW spectral dataset was determined to be 3LVs (Figure 3).

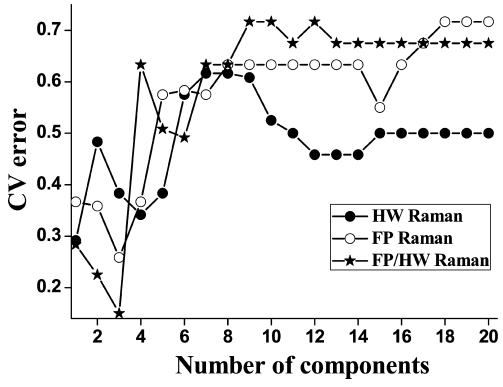

Figure 3. The relationship between the number of PLS components (LVs) and the cross-validation error for correct classification of normal and cervical dysplasia using FP, HW, and the integrated FP/HW tissue Raman spectroscopy, respectively.

Figure 4 shows the diagnostically significant LV loadings ($p < 0.005$) for the integrated FP/HW spectral dataset, accounting for

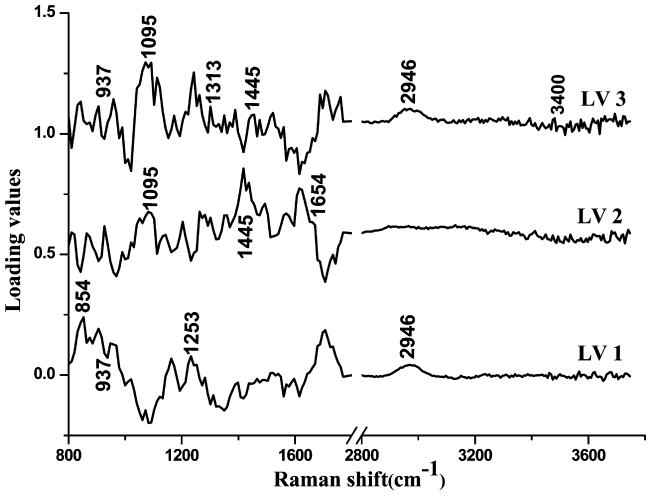

Figure 4. PLS component (LV) loadings in the developed PLS-DA model. The first three diagnostically significant LVs (LV1, 24.03%; LV2, 10.73%; and LV3, 4.01%) accounting for ~38.77% of the total variance were calculated from the in vivo integrated FP/HW Raman spectra of cervical tissue, uncovering the diagnostically relevant spectral features for precancer classification. Each loading is shifted vertically for better visualization. The broken interval (—//—) indicates the region of ~1800−2800 cm^{-1} that does not contain much tissue biochemical information.

38.77% (LV1, 24.03%; LV2, 10.73%; and LV3, 4.01%) of the total Raman spectral variations, which typically represent the spectral variations around the major Raman peak positions (854, 1095, 1253, 1313, 1445, 1654, 2946, and 3400 cm^{-1}). Figures 5a−c show the box charts of significant LV scores obtained from the integrated FP/HW spectral dataset to visualize the different degrees of diagnostic utility of significant LVs for dysplasia classification. For instance, LV2 shows the greatest efficacy in differentiating cervical dysplasia than other LVs.

Figure 6 shows the cross-validated prediction results (posterior probabilities) belonging to normal and cervical precancer tissue as calculated for (a) FP, (b) HW, and (c) integrated FP/HW datasets, respectively. The threshold lines in the posterior probability scatter plots yield diagnostic accuracies of 80.3% (382/476), 74.2% (353/476), and 82.6% (393/476) (sensitivities of 84.2% (101/120), 76.7% (92/120), and 85.0% (102/120), respectively; and specificities of 78.9% (281/356), 73.3% (261/356), and 81.7% (291/356) (Table 2)), respectively, confirming that the integrated FP/HW confocal Raman spectroscopy is the most robust for in vivo diagnosis of cervical dysplasia. The ROC curves (Figure 7) are also generated for the three spectral datasets (FP, HW, and the integrated FP/HW) to further evaluate the groups separation. The integration areas under the ROC curves are 0.88, 0.78, and 0.92 for FP, HW, and the integrated FP/HW Raman spectroscopy, respectively, substantiating the efficacy of the integrated FP/HW confocal Raman spectroscopy for improving dysplastic classification as compared to FP or HW spectroscopy alone.

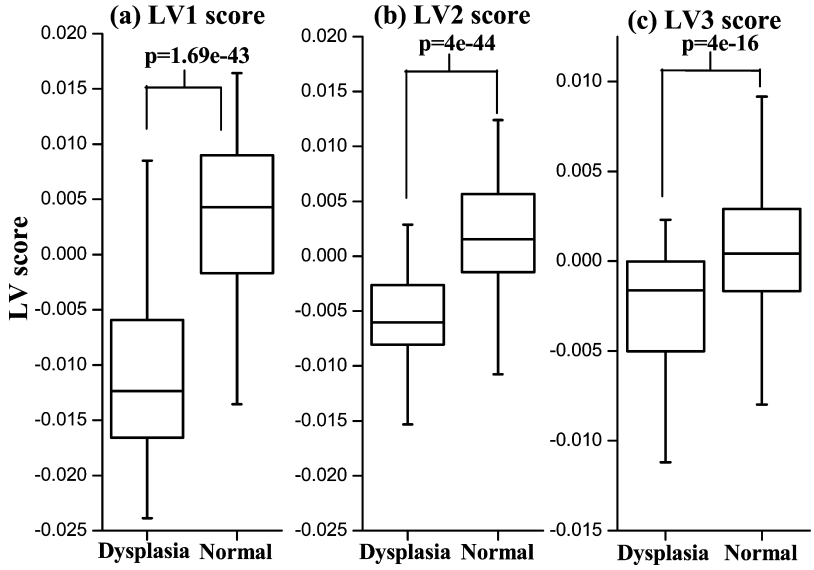

Figure 5. Box charts of the three significant PLS component (LV) scores calculated from the in vivo integrated FP/HW Raman dataset for normal and dysplastic cervical tissue types: (a) LV1 score, (b) LV2 score, and (c) LV3 score. The line within each box represents median, while the lower and upper boundary of the box indicate the first (25th percentile) and the third (75th percentile) quartiles, respectively. Whiskers (error bars) represent 1.5-fold interquartile range. The *p*-values of unpaired two-sided Student's *t*-test ($p < 0.005$) on the LVs of normal and precancer cervical tissues are shown.

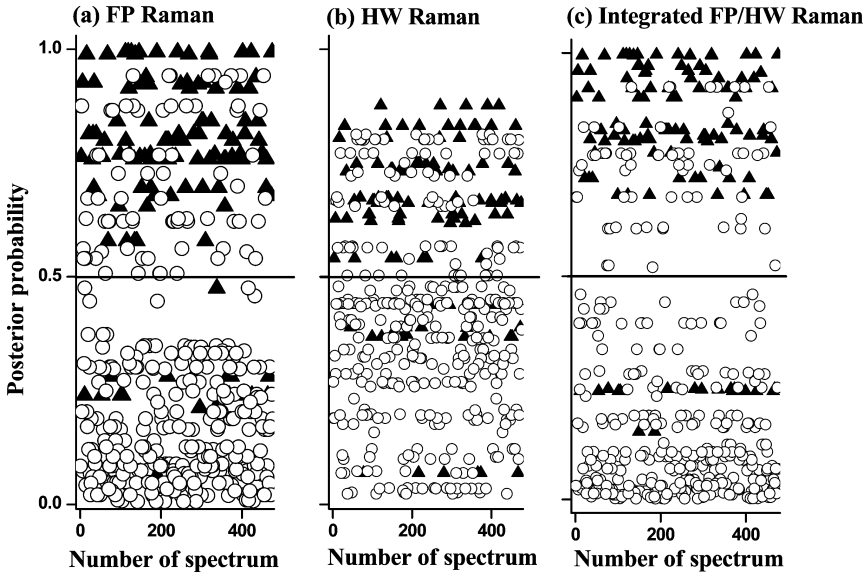

Figure 6. Scatter plots of the posterior probability values belonging to the normal and precancer cervical tissue categories calculated from (a) FP, (b) HW and (c) integrated FP/HW Raman spectra, respectively, using the PLS-DA together with leave-one-patient-out, cross-validation method. The dotted line gives the sensitivities of 84.2% (101/120), 76.7% (92/120), and 85.0% (102/120), respectively; specificities of 78.9% (281/356), 73.3% (261/356), and 81.7% (291/356), respectively, for separating dysplasia from the normal cervical tissue using FP, HW, and integrated FP/HW Raman spectra. ((▲) Precancer (n = 120), (○) normal (n = 356).)

Table 2. Comparison of Diagnostic Performance of Different Raman Techniques (FP, HW, and the Integrated FP/HW) for Differentiating Dysplasia from Normal Cervical Tissue In Vivo

Raman spectroscopic modalities	retained LVs	sensitivity (%)	specificity (%)	accuracy (%)
fingerprint (FP) (800−1800 cm^{-1})	3	84.2 (101/120)	78.9 (281/356)	80.3 (382/476)
high wavenumber (HW) (2800−3700 cm^{-1})	1	76.7 (92/120)	73.3 (261/356)	74.2 (353/476)
integrated FP/HW	3	85.0 (102/120)	81.7 (291/356)	82.6 (393/476)

4. DISCUSSION

Cyto-histopathologic correlation (colposcope-guided biopsies due to cytological abnormality) for cervical precancer diagnosis relies on cytological and morphological alterations within the cells and tissue.[32] These guided clinical diagnostic techniques are subjective and prone to considerable intraobserver and interobserver disagreements, leading to extensive research in optical diagnostics (i.e., optical biopsy) of precancer and cancer. Recent researches based on optical diagnostics of diseases have

dx.doi.org/10.1021/ac300394f | *Anal. Chem.* 2012, 84, 5913−5919

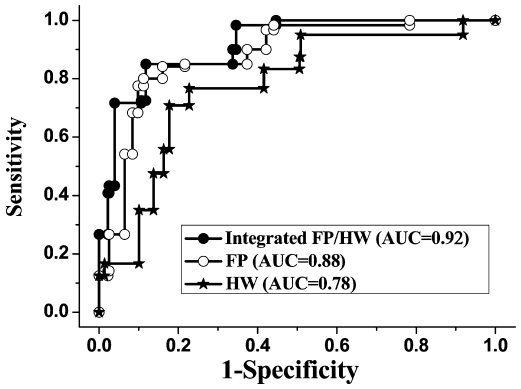

Figure 7. Receiver operating characteristic (ROC) curves of discrimination results for in vivo FP, HW, and integrated FP/HW Raman spectra, respectively, for cervical precancer tissue classification through the use of Raman spectroscopy and PLS-DA together with the leave-one-patient-out, cross-validation method. The integrated area under the ROC curves are 0.88, 0.78, and 0.92 for the FP, HW and integrated FP/HW Raman spectra, respectively, illustrating the best performance of integrated FP/HW confocal Raman spectroscopy for in vivo cervical precancer diagnosis during clinical colposcopy.

been directed toward Raman spectral diagnostics that can provide FP information about the changes of biochemical structures and compositions of tissue for molecular discrimination of precancer and cancer.[9−12,16] Current Raman studies have evaluated tissue Raman spectra mostly either in the FP[9−12,16,17] or HW[14,20,21,23,33,34] region. Only a very limited amount of work has reported the Raman measurements from both the FP and HW regions,[23] but the Raman signals are measured either by successively switching the different excitation laser lines or by rotating the gratings for each individual region,[18,23] which are very time-consuming and not suited for rapid in vivo disease diagnostics in clinical settings. For example, Chau et al.[23] utilized a 830-nm excitation laser for FP Raman spectral acquisition, and then switched to another 740-nm excitation laser for HW Raman spectral acquisition. In this work, we have developed an integrated FP/HW confocal Raman diagnostic system for simultaneous acquisition of FP/HW Raman signals of the cervix in vivo within 1 s during clinical colposcopic inspections. Our Monte Carlo simulations show that the confocal Raman probe with a ball lens developed can selectively collect the Raman photons from the depth of ∼160 μm in the cervix,[24] while much reduce the tissue autofluorescence collection originating from the deeper stromal tissue, compared to the volume fiber-optic Raman probe design.[16,35]

We further employed PLS-DA methodology to explore the diagnostic utility of the integrated FP/HW confocal Raman spectroscopy for improving in vivo diagnosis of cervical precancer. The PLS-DA modeling of FP Raman spectra is able to extract diagnostically significant Raman spectral features (LV1, 24.03%; LV2, 10.73%; and LV3, 4.01%), resolving highly specific tissue biomolecular information in the FP region (854, 1095, 1253, 1313, 1445, and 1654 cm^{-1}). Specifically, the tissue Raman spectra showed reduced glycogen and proteins (854 and 1654 cm^{-1}), and the increased nuclear content (1095 cm^{-1}) with dysplastic progression in the cervix. The decreased glycogen and structural proteins (elastin and collagen) were mainly related to the loss of differentiation in the cervical epithelial cells during neoplastic progression and the existence of structural proteins in the cervix,[3,18] whereas the increased nuclear content (1095 cm^{-1}) indicated the elevated number of epithelial cells associated with dysplastic progression in the cervix. The amide I (1654 cm^{-1}) was also noticeably decreased with dysplastic transformation.[36] Thus, FP Raman spectroscopy associated with PLS-DA modeling using 3LVs provides highly specific signatures of various biomolecules, enabling in vivo identification of tissue pathology in the cervix.

On the other hand, the PLS-DA modeling of HW Raman spectra is able to determine the significant Raman diagnostic information (LV1, 27.99%) mainly associated with protein and water changes with dysplastic transformation. The biochemical basis of HW Raman spectra associated with cervical precancer progression has been discussed elsewhere.[21] In short, the dysplastic Raman spectra showed significantly reduced protein (2946 cm^{-1}, CH_3 stretching of proteins) and increased tissue water content (3100−3700 cm^{-1} broad OH band). The low protein content (2946 cm^{-1}) could be attributed to significant reduction in collagen Raman signals (i.e., from stroma) due to thickening of epithelium with dysplastic transformation; while the high tissue water content is likely related to an increase of certain types of aquaporins (AQP) in the dysplastic cervical cells.[14,21] The HW tissue Raman spectroscopy based on PLS-DA modeling (1LV) rendered a diagnostic accuracy of 74.2% (353/476) (sensitivity of 76.7% (92/120) and specificity of 73.3% (261/356)) for in vivo cervical precancer detection. Further, the PLS-DA modeling of the integrated FP/HW Raman spectra rendered intricate 3 LVs (LV1, 24.03%; LV2, 10.73%; and LV3, 4.01%), revealing the diagnostic features in both FP and HW regions for in vivo tissue diagnosis and characterization (see Figure 4). Hence, the integrated FP/HW Raman spectroscopy provides the best diagnostic accuracy of 82.6% (393/476) (sensitivity of 85.0% (102/120) and specificity of 81.7% (291/356)) for improving in vivo precancer diagnosis, compared to either FP or HW Raman spectroscopy alone (see Figure 6). The complementary nature of both Raman spectral modalities for enhancing tissue diagnosis and characterization can be explained by backtracking the misclassified cases of each Raman spectral modality. The FP and HW Raman spectroscopy misclassified 94 and 123 spectra, respectively, from 21 patients of the total 44 patients recruited, in which 5 misclassified patients were identical in the both the modalities. However, the integration of these two Raman modalities reduced the number of misclassified patients to 11 (83 spectra), whereby 4 patients were identical for both Raman regions. The result demonstrates that combining the FP and HW Raman spectral modality can largely reduce the misclassification of nonidentical patients, confirming the addition of complementary spectral information required for enhancing precancer diagnosis. For instance, the change of water content of cervical tissue with dysplastic progression is reflected in the HW region, but not in the FP region. The ROC curves (see Figure 7) further validate the best performance and robustness of the integrated FP/HW Raman spectroscopy for in vivo cervical precancer detection at colposcopy. This work suggests that by fully utilizing the complementary Raman spectral signatures in FP and HW regions, the integrated FP/HW Raman spectroscopy can be a novel and sensitive diagnostic means for improving the identification of early pathologic changes (e.g., dysplasia) in the cervix at the molecular level.

5. CONCLUSION

We report for the first time (to the best of our knowledge) the utilization of simultaneous FP/HW confocal Raman spectroscopy developed for in vivo diagnosis of cervical precancer. This study discloses that fingerprint (FP) and high wavelength (HW)

Raman spectroscopic techniques are complementary, and the integration of the two complementary Raman spectroscopic techniques further improves in vivo cervical precancer detection. It is expected that the simultaneous FP/HW confocal Raman spectroscopy could become a promising clinical diagnostic tool for enhancing real-time in vivo diagnosis and characterization of cervical precancer and cancer at colposcopy.

AUTHOR INFORMATION

Corresponding Author

*Tel.: +65-6516-8856. Fax: +65-6872-3069. E-mail: biehzw@nus.edu.sg.

Notes

The authors declare no competing financial interest.

ACKNOWLEDGMENTS

This work was supported by the Biomedical Research Council, and the National Medical Research Council, Singapore.

REFERENCES

(1) Parkin, D. M.; Bray, F.; Ferlay, J.; Pisani, P. *Int. J. Cancer* **2001**, *94*, 153−156.

(2) Parkin, D. M.; Bray, F.; Ferlay, J.; Pisani, P. *Cancer J. Clin.* **2005**, *55*, 74−108.

(3) Lyng, F.; Faoláin, E.; Conroy, J.; Meade, A.; Knief, P.; Duffy, B.; Hunter, J.; Byrne, M.; Kelehan, P.; Byrne, H. *Exp. Mol. Pathol.* **2007**, *82*, 121−129.

(4) Freeberg, J. A.; Benedet, J. L.; MacAulay, C.; West, L. A.; Follen, M. *Gynecol. Oncol.* **2007**, *107*, S248−S255.

(5) Arbyn, M.; Sankaranarayanan, R.; Muwonge, R.; Keita, N.; Dolo, A.; Mbalawa, C. G.; Nouhou, H.; Sakande, B.; Wesley, R.; Somanathan, T. *Int. J. Cancer* **2008**, *123*, 153−160.

(6) Mirabal, Y. N.; Chang, S. K.; Atkinson, E. N.; Malpica, A.; Follen, M.; Richards-Kortum, R. *J. Biomed. Opt.* **2002**, *7*, 587−594.

(7) Wong, P. T. T.; Wong, R. K.; Fung, M. F. K. *Appl. Spectrosc.* **1993**, *47*, 1058−1063.

(8) Ramanujam, N.; Mahadevan, A.; Thomsen, S.; Silva, E.; Richards-Kortum, R. *Gynecol. Oncol.* **1994**, *52*, 31−38.

(9) Mahadevan-Jansen, A.; Follen, M.; Ramanujam, N.; Malpica, A.; Thomsen, S.; Utzinger, U.; Richards-Kortum, R. *Photochem. Photobiol.* **1998**, *68*, 123−132.

(10) Duraipandian, S.; Zheng, W.; Ng, J.; Low, J. J. H.; Ilancheran, A.; Huang, Z. *Analyst* **2011**, *136*, 4328−4336.

(11) Teh, S. K.; Zheng, W.; Ho, K. Y.; Teh, M.; Yeoh, K. G.; Huang, Z. *J. Raman Spectrosc.* **2009**, *40*, 908−914.

(12) Huang, Z.; McWilliams, A.; Lui, H.; McLean, D. I.; Lam, S.; Zeng, H. *Int. J. Cancer* **2003**, *107*, 1047−1052.

(13) Almond, L. M.; Hutchings, J.; Shepherd, N.; Barr, H.; Stone, N.; Kendall, C. *J. Biophotonics* **2011**, *4*, 685−695.

(14) Duraipandian, S.; Zheng, W.; Ng, J.; Low, J. J. H.; Ilancheran, A.; Huang, Z. *Proc. SPIE* **2012**, *8214*, 82140A (1−6).

(15) Utzinger, U.; Heintzelman, D. L.; Mahadevan-Jansen, A.; Malpica, A.; Follen, M.; Richards-Kortum, R. *Appl. Spectrosc.* **2001**, *55*, 955−959.

(16) Bergholt, M. S.; Zheng, W.; Lin, K.; Ho, K. Y.; Teh, M.; Yeoh, K. G.; So, J. B. Y.; Huang, Z. *Technol. Cancer Res. Treat.* **2011**, *10*, 103−112.

(17) Teh, S. K.; Zheng, W.; Ho, K. Y.; Teh, M.; Yeoh, K. G.; Huang, Z. *Br. J. Cancer* **2008**, *98*, 457−465.

(18) Kamemoto, L. E.; Misra, A. K.; Sharma, S. K.; Goodman, M. T.; Luk, H.; Dykes, A. C.; Acosta, T. *Appl. Spectrosc.* **2010**, *64*, 255−261.

(19) Koljenovic, S.; Schut, T. C. B.; van Meerbeeck, J. P.; Maat, A. P. W. M.; Burgers, S. A.; Zondervan, P. E.; Kros, J. M.; Puppels, G. J. *J. Biomed. Opt.* **2004**, *9*, 1187−1197.

(20) Koljenovic, S.; Schut, T. C. B.; Wolthuis, R.; de Jong, B.; Santos, L.; Caspers, P. J.; Kros, J. M.; Puppels, G. J. *J. Biomed. Opt.* **2005**, *10*, 031116−031111.

(21) Mo, J.; Zheng, W.; Low, J. J. H.; Ng, J.; Ilancheran, A.; Huang, Z. *Anal. Chem.* **2009**, *81*, 8908−8915.

(22) García-Flores, A.; Raniero, L.; Canevari, R.; Jalkanen, K.; Bitar, R.; Martinho, H.; Martin, A. *Theor. Chim. Acta* **2011**, *130*, 1231−1238.

(23) Chau, A. H.; Motz, J. T.; Gardecki, J. A.; Waxman, S.; Bouma, B. E.; Tearney, G. J. *J. Biomed. Opt.* **2008**, *13*, 040501.

(24) Mo, J.; Zheng, W.; Huang, Z. *Biomed. Opt. Express* **2010**, *1*, 17−30.

(25) Sankaranarayanan, R.; Wesley, R.; Somanathan, T.; Dhakad, N.; Shyamalakumary, B.; Amma, N. S.; Parkin, D. M.; Nair, M. K. *Cancer* **1998**, *83*, 2150−2156.

(26) Zhao, J.; Lui, H.; McLean, D. I.; Zeng, H. *Appl. Spectrosc.* **2007**, *61*, 1225−1232.

(27) Hedegaard, M.; Krafft, C.; Ditzel, H. J.; Johansen, L. E.; Hassing, S.; Popp, J. *Anal. Chem.* **2010**, *82*, 2797−2802.

(28) De Lucia, J. F. C.; Gottfried, J. L.; Munson, C. A.; Miziolek, A. W. *Appl. Opt.* **2008**, *47*, G112−G121.

(29) Stone, N.; Kendall, C.; Smith, J.; Crow, P.; Barr, H. *Faraday Discuss.* **2004**, *126*, 141−157.

(30) Movasaghi, Z.; Rehman, S.; Rehman, I. U. *Appl. Spectrosc. Rev.* **2007**, *42*, 493−541.

(31) Robichaux-Viehoever, A.; Kanter, E.; Shappell, H.; Billheimer, D.; Jones, H., III; Mahadevan-Jansen, A. *Appl. Spectrosc.* **2007**, *61*, 986−993.

(32) Teh, S. K.; Zheng, W.; Ho, K. Y.; Teh, M.; Yeoh, K. G.; Huang, Z. *Int. J. Cancer* **2010**, *126*, 1920−1927.

(33) Santos, L. F.; Wolthuis, R.; Koljenovic, S.; Almeida, R. M.; Puppels, G. J. *Anal. Chem.* **2005**, *77*, 6747−6752.

(34) Lin, K.; Lau, D.; Huang, Z. *Biosensors and Bioelectronics* **2012**, *35*, 213−217.

(35) Huang, Z.; Teh, S. K.; Zheng, W.; Mo, J.; Lin, K.; Shao, X.; Ho, K. Y.; Teh, M.; Yeoh, K. G. *Opt. Letts.* **2009**, *34* (6), 758−760.

(36) Jess, P. R. T.; Smith, D. D. W.; Mazilu, M.; Dholakia, K.; Riches, A. C.; Herrington, C. S. *Int. J. Cancer* **2007**, *121*, 2723−2728.

NOTE ADDED AFTER ASAP PUBLICATION

Due to a production error, this paper was published on the Web on June 20, 2012 with an error in the Abstract. The revised version was reposted on June 27, 2012.